AD-A191 905 AN OPTIMIZATION METHOD FOR THE REDUCTION OF PROPELLER 1/1
UNSTEADY FORCES(U) NAVAL OCEAN SYSTEMS CENTER SAN DIEGO
CA T S MAUTNER FEB 88

UNCLASSIFIED F/G 20/1 NL

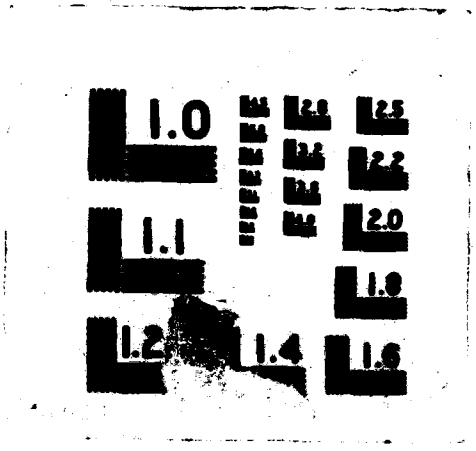
1.0
1.1
1.2
1.4
2.0
1.8
1.6

UNCLAS
SECURITY

AD-A191 905

DTIC FILE COPY

DOCUMENTATION PAGE

1a. REPORT SECURITY CLASSIFICATION UNCLASSIFIED	1b. RESTRICTIVE MARKINGS
2a. SECURITY CLASSIFICATION AUTHORITY	3. DISTRIBUTION/AVAILABILITY OF REPORT
2b. DECLASSIFICATION/DOWNGRADING SCHEDULE	Approved for public release; distribution is unlimited.
4. PERFORMING ORGANIZATION REPORT NUMBER(S)	5. MONITORING ORGANIZATION REPORT NUMBER(S)
6a. NAME OF PERFORMING ORGANIZATION Naval Ocean Systems Center 6b. OFFICE SYMBOL (If applicable) NOSC	7a. NAME OF MONITORING ORGANIZATION Naval Ocean Systems Center
6c. ADDRESS (City, State and ZIP Code) San Diego, California 92152-5000	7b. ADDRESS (City, State and ZIP Code) San Diego, California 92152-5000
8a. NAME OF FUNDING/SPONSORING ORGANIZATION Naval Underwater Systems Center 8b. OFFICE SYMBOL (If applicable) NUSC	9. PROCUREMENT INSTRUMENT IDENTIFICATION NUMBER
8c. ADDRESS (City, State and ZIP Code) Newport, RI 02841	10. SOURCE OF FUNDING NUMBERS PROGRAM ELEMENT NO.: 62633N PROJECT NO.: HM35 TASK NO.: SF33321 AGENCY ACCESSION NO.: DN305 123

11. TITLE (Include Security Classification)

An Optimization Method for the Reduction of Propeller Unsteady Forces

12. PERSONAL AUTHOR(S)

T.S. Mautner

13a. TYPE OF REPORT	13b. TIME COVERED	14. DATE OF REPORT (Year, Month, Day)	15. PAGE COUNT
Professional paper/speech	FROM Jan 1988 TO Jan 1988	February 1988	

16. SUPPLEMENTARY NOTATION

17. COSATI CODES			18. SUBJECT TERMS (Continue on reverse if necessary and identify by block number)
FIELD	GROUP	SUB-GROUP	propeller geometry wake-adapted propellers harmonic components

19. ABSTRACT (Continue on reverse if necessary and identify by block number)

Based on the work of Greenblatt (1978), an enhanced optimization technique for the reduction of propeller unsteady forces and the determination of skew distributions has been developed. The current method provides an efficient propeller design tool capable of determining a variety of cubic or quadratic skew distributions, subject to constraints, which minimize the unsteady forces produced by the various harmonic components of the input wake. The original skew optimization method was extended to include higher order harmonics, and the original force calculation method was replaced by an extended version of the method developed by Thompson (1976). Calculation of forces and skew distributions associated with a representative propeller show that acceptable reduction of unsteady forces can be obtained without having to place severe restrictions on the model constraints.

cont'd pg 1 →

Presented at the AIAA 26th Aerospace Sciences Meeting, 11-14 January 1988, Reno, NV.

20. DISTRIBUTION/AVAILABILITY OF ABSTRACT	21. ABSTRACT SECURITY CLASSIFICATION
☐ UNCLASSIFIED/UNLIMITED ☒ SAME AS RPT ☐ DTIC USERS	UNCLASSIFIED
22a. NAME OF RESPONSIBLE INDIVIDUAL T.S. Mautner	22b. TELEPHONE (Include Area Code) (619) 553-1588
	22c. OFFICE SYMBOL Code 634

DD FORM 1473, 84 JAN

83 APR EDITION MAY BE USED UNTIL EXHAUSTED
ALL OTHER EDITIONS ARE OBSOLETE

UNCLASSIFIED
SECURITY CLASSIFICATION OF THIS PAGE

AIAA'88

AIAA-88-0265
An Optimization Method for the Reduction of Propeller Unsteady Forces

T.S. Mautner, Naval Ocean Systems Center, San Diego, CA

AIAA 26th Aerospace Sciences Meeting
January 11-14, 1988/Reno, Nevada

AN OPTIMIZATION METHOD FOR THE REDUCTION OF PROPELLER UNSTEADY FORCES

Thomas S. Mautner
Naval Ocean Systems Center
San Diego, CA 92152

ABSTRACT

Based on the work of Greenblatt (1978), an enhanced optimization technique for the reduction of propeller unsteady forces and the determination of skew distributions has been developed. The current method provides an efficient propeller design tool capable of determining a variety of cubic or quadratic skew distributions, subject to constraints, which *minimize* the unsteady forces produced by the various harmonic components of the input wake. The original skew optimization method was extended to include higher order harmonics, and the original force calculation method was replaced by an extended version of the method developed by Thompson (1976). Calculation of forces and skew distributions associated with a representative propeller show that acceptable reduction of unsteady forces can be obtained without having to place severe restrictions on the model constraints.

NOMENCLATURE

a_m , b_m	Fourier coefficients
A_j	Polynomial coefficients
A_k	Multiplicative factor
A_F	Vehicle frontal area
c_m or c_n	Fourier coefficient magnitude = $(a_m^2 + b_m^2)^{1/2}$
c^*	Complex Fourier coefficient = $a_m - ib_m$
C	Propeller blade chord length
C_D	Vehicle drag coefficient = Drag/$\frac{1}{2}\rho V_s^2 A_F$
C_L	Blade section lift coefficient
C_P	Phase angle = $\tan^{-1}(a_m/b_m)$
C_Q	Torque coefficient = Torque/$\frac{1}{2}\rho V_s^2 \pi R^3$
C_T	Thrust coefficient = Thrust/$\frac{1}{2}\rho V_s^2 \pi R^2$
D	Propeller diameter
F_c	Cost function
F_x , F_y	Unsteady side forces
$F_s^{(m)}$	Total unsteady side force for the m-th harmonic
$F_x^{(m)}$	Unsteady thrust for the m-th harmonic
G	Constraint function
Im	Imaginary part of a complex function
j	Index taking on values = 1,.....P
J	Advance ratio = $\pi V_s / \Omega R$
k	The reduced frequency = $\omega C \omega / V_s$
K(k)	Sears' function
L	Lift force on a airfoil/blade section
m	Order of the propeller force harmonic
M	Moment/Torque on a blade element
n	Index taking on values = mN_b
N_b	Number of propeller blades
P	Number of blade elements having width Δr
PC	Propulsive coefficient = (Thrust · V_s)/(Torque · Ω)
Pc	Penalty function
r	Radial coordinate
r_h	Hub radius
r_s	Starting radius of the skew distribution
r_t	Propeller tip radius
Δr_j	Width of the j th blade element
R	Propeller radius
R_B	Body radius
Re	Real part of a complex function
S_s	Starting slope of the skew distribution
S_t	Skew distribution slope at the propeller tip
t	Time
T_x , T_y	Unsteady moments
$T_s^{(m)}$	Total unsteady moment for the m th harmonic
$T_x^{(m)}$	Unsteady torque for the m th harmonic
T(k)	Horlock's function
V	Velocity
V_s	Free stream velocity or vehicle speed
V_{tip}	Propeller blade tip speed
V_{ri}	Nondimensional, resultant relative velocity of blade section and fluid
W	Weighting function
W_R	Ratio W(m=12)/W(m=24)
x,y,z	Rectangular coordinates
$\bar{r}$	Radial position = $(r-r_h)/(R-r_h)$
$\underline{X}$	Vector in parameter space
α	Angle of attack of a blade element
β	Blade section pitch angle (radians)
η_j	Propeller blade spacing = $2\pi j/N_b$
ω	Frequency
Ω	Angular velocity of the propeller
ϕ_{ij}	Phase shift = $\psi_j + \eta_i$
ψ	Mid-Chord skew angle
ψ_t	Mid-Chord skew angle at the propeller tip
ρ	Fluid density
σ	Cavitation number based on free stream static pressure and velocity
τ	Propeller thrust deduction factor
θ	Angular coordinate in the direction of propeller rotation

INTRODUCTION

One current and important issue in the design of both marine and aircraft propellers is the reduction of propulsor generated noise. In general, propeller designers are concerned with the reduction of noise due to both the transmission of unsteady propeller forces through shafting into the vehicle and propeller noise radiated into the near and far fields. For example, the reduction of self-noise in a marine vehicle will result in improved sensor operation while the reduction of aircraft noise improves cabin comfort and reduces ground noise.

The problem considered herein is the generation of propeller noise due to non-uniform inflow velocity fields. This has been and still is an issue of research in the area of marine propellers, and it is felt that a recently developed method of calculating unsteady forces and specifying skew distributions (i.e. blade sweep) for marine propellers may also be applicable in the design and analysis of aircraft propellers, in particular pusher propellers. Although the sources of the flow non-uniformities may be somewhat different for marine and aircraft propellers, flow non-uniformities will result in the generation of unsteady forces and noise irregardless of the propeller type. For example, a propeller operating on an axisymmetric body with appendages (a typical underwater case) experiences a non-uniform inflow velocity field due to the upstream appendages (for example Nelson and Fogarty, 1977) while an aircraft prop-fan is subjected to flow non-uniformities due to the wing installation, the nacelle or engine exhaust and a pusher propeller is exposed to a non-uniform flow field due to the upstream airframe geometry (for examples see Metzger, 1984; Schulten, 1984; Metzger and Rohrbach, 1986; and Takallu and Block 1987).

The generation of unsteady propeller blade forces can be described by consideration of a propeller operating in the turbulent wake of a body having upstream protuberances which create wake non-uniformities which in turn result in spatial and temporal fluctuations of blade angle-of-attack. These angle-of-attack fluctuations result in unsteady blade loadings and the generation of propeller noise, and the noise sources are characterized by three types of unsteady force mechanisms: a) turbulence injestion; b) vortex shedding; and c) blade-rate. The first two mechanisms typically generate continuous spectrum (broadband) radiated noise while blade-rate forces generate discrete frequency noise at various blade-passage frequencies and harmonics. This paper will address the reduction of blade-rate noise which provided the original motivation for the application of skew in propeller design.

An example of a non-uniform wake incident upon a propeller is one generated by an axisymmetric body with appendages. The boundary layer behind the appendage (i.e. figure 1) is characterized by a complex velocity field typically having velocity excesses at inner radii and velocity defects at the outer radii. This type of velocity field has a complex harmonic content distribution and its effect on blade-rate noise cannot be predicted without detailed examination of the wake and the radial distribution of propeller blade forces.

Techniques are available for computing unsteady forces and skew distributions, and these methods range from low-aspect ratio approximations to unsteady airfoil theory to complete unsteady, lifting-surface methods. However, since no method was available to systematically determine an optimum skew distribution for the reduction of unsteady forces, the propeller skew optimization program SKEWOPT (Greenblatt, 1978; and Parsons and Greenblatt, 1978) was developed. SKEWOPT determines a quadratic or cubic skew distribution using an optimization technique which finds the set of parameters for which a user-defined linear combination of the unsteady force and moment amplitudes are minimized. SKEWOPT was written for use in ship propeller design; however, the intention was that, after minor modifications such as the inclusion of higher order harmonic groups, it would be suitable for torpedo and submarine propeller design. Since the force calculation method in SKEWOPT was not sufficiently documented, the method was replaced, and, due to the difficulties encountered in modifying SKEWOPT, a new program (SKEWOPT-2), patterned after SKEWOPT, was written.

In the following discussion, the method used in SKEWOPT-2 for determining the optimum skew distribution for a propeller operating on an axisymmetric body with upstream control surfaces will be described. The method optimizes the skew (combination of warp and rake) such that the unsteady propeller blade-rate forces are minimized. The forward propeller of a counterrotating propeller set will be used to demonstrate use of the method. While the discussion and results presented deal specifically with a marine propeller application, it is felt that the method is applicable to any propeller operating in a non-uniform inflow velocity field.

THE SKEW OPTIMIZATION PROBLEM

VELOCITY FIELD

In the design of wake-adapted propellers, it is important that the inflow velocity distribution be properly specified. The state-of-the-art in boundary layer computations is such that the inflow velocity field, for a body having appendages located upstream of the propulsor, should be determined experimentally. Even though circumferentially averaged velocity profiles are sufficient for propeller design calculations, the calculation of unsteady forces requires that both the radial and circumferential distributions of the wake be considered.

The velocity data used in this study was obtained from wind tunnel tests conducted in the Northrop (NORAIR) subsonic wind tunnel located in Hawthorne, California (see Nelson and Fogarty, 1977). In order to obtain body drag measurements, the 0.6 scale model was strut mounted in such a manner to reduce horizontal buoyancy effects, and the tests were conducted over a Reynolds number range of $1.3-2.4\times10^6$ per foot. The boundary layer measurements were made using a pair of pitot tube rakes. One rake contained four static pressure tubes and the second rake had eight total head tubes. To avoid the effects of the strut, wake measurements were made over an arc slightly larger than 90° on the upper side of the body, and the center of the measurement arc coincides with the fin's trailing edge (body had four identical fins).

The measured wake data, shown in figure 1, exhibits the velocity excesses at the inner radii and the velocity deficits at the outer radii, produced by both viscous and potential effects, typically found behind an appendage on an axisymmetric body. The velocity excesses are due to the horseshoe vortex formed at the appendage/body intersection, and the velocity deficits at the outer radii are due to the fin's tip vortex (see, for example, Greeley and Milewski, 1986).

Velocity fields of this type play an important part in the design of wake-adapted propellers because the spatial variations result in the generation of unsteady forces. The velocity data in figure 1 represents a time averaged, spatially varying field, and since the spatial velocity distribution is periodic and continuous, it may be represented in terms of a Fourier series. For example, the axial component of the velocity, at a position (r,ϑ), can be expressed as

$$\frac{V(r,\vartheta)}{V_s} = \frac{a_0(r)}{2} + \sum_{m=1}^{\infty}\left[a_m(r)\cos(m\vartheta) + b_m(r)\sin(m\vartheta)\right] = \mathrm{Re}\left\{\frac{a_0}{2} + \sum_{m=1}^{\infty}\left[a_m(r) - ib_m(r)\right]\exp(im\vartheta)\right\} \tag{1}$$

where Re( ) denotes the real part, and the Fourier coefficients are defined by

$$a_0(r) = \frac{1}{\pi}\int_{-\pi}^{\pi}\frac{V}{V_s}\,d\vartheta$$

$$a_m(r) = \frac{1}{\pi}\int_{-\pi}^{\pi}\frac{V}{V_s}\cos(m\vartheta)\,d\vartheta \tag{2}$$

$$b_m(r) = \frac{1}{\pi}\int_{-\pi}^{\pi}\frac{V}{V_s}\sin(m\vartheta)\,d\vartheta$$

Since, the term $a_0(r)$ does not vary in ϑ, it is associated with the steady state thrust and torque, and the additional terms are sinusoidal fluctuations of the inflow velocity which produce the unsteady forces and moments.

PROPELLER GEOMETRY

The propeller geometry chosen for the present study is that for the forward propeller of a counterrotating propeller set designed using the method developed by Nelson (1972, 1975). The design utilized the circumferential mean, inflow velocity field measured by Nelson and Fogarty (1977) and the parameters given in table 1. The propeller geometry, shown schematically in figure 2, was determined using the lifting-line portion of Nelson's design method. The calculated performance parameters for the counterrotating propeller set are given in table 1 while the details of the forward propeller geometry are given in table 2.

Once the velocity field and propeller geometry are determined, the problem of determining an "optimum" skew distribution requires the formulation of a nonlinear programming problem which includes an unsteady force calculation method. First, the calculation of the unsteady forces will be considered.

UNSTEADY FORCE CALCULATION METHOD

During the skew optimization process, unsteady forces will be calculated many times, therefore, it would be desirable to use an efficient, inexpensive method. The original version of SKEWOPT (Greenblatt, 1978) had both a two-dimensional, unsteady and a more time consuming lifting-line method available to calculate the forces. To overcome both documentation and computation problems, the original SKEWOPT force calculation methods were replaced by a method developed by Thompson (1976). His method divides the propeller blade into strips which are considered two-dimensional airfoils. Included in the method are: a) the two-dimensional unsteady airfoil theories of Sears (1941) and Horlock (1968) which allow consideration of sinusoidal velocity fluctuations normal and parallel to the inflow velocity; and b) corrections to the blade lift force due to the presence of adjacent propeller blades. The method has been extended to include the effects of camber using the method of Naumann and Yeh (1973) and to calculate the total force and moment on the propeller. A brief description of the method follows (for details of the method see: Thompson, 1976; Mautner, 1987b; and Mautner and Blaisdell, 1987)

Expressions for the unsteady lift acting on a two-dimensional airfoil due to a periodically varying free stream velocity were developed by Sears (1941) and Horlock (1968). They assumed that the airfoil can be represented by an isolated flat plate, and that the flow is incompressible, inviscid and irrotational except for surfaces of distributed singularities. The airfoil is replaced by a distribution of vortices, and the shed vorticity is assumed to lie on a line parallel to the unsteady free stream velocity. Also, the inflow velocity and the velocity induced by the vortex system must satisfy the boundary condition that there is no flow through the plate. Their formulation results in an integral equation describing the vortex distribution, and the solution of the integral equation yields the total velocity on the plate's surface. Using Bernoulli's equation, the pressure distribution on the upper and lower surfaces of the plate are obtained, and the unsteady lift is determined from the pressure difference.

In order to apply two-dimensional, unsteady airfoil theory to propellers, the propeller blade is divided into strips of width Δr_j as indicated in figure 2. Each blade element is then treated as an isolated two-dimensional airfoil having at its mid-point the relative velocity V_{rj}. The velocities which determine V_{rj} are the propeller rotation Ωr_j , the mean axial inflow velocity $V_j(r,\beta)$ and the down wash velocity (which for wake-adapted propellers includes induced and interference velocities). The resulting angle between Ωr_j and V_{rj} defines the local pitch angle β_j.

The varying axial velocity field incident upon the rotating blade row is resolved into components normal and parallel to V_{rj} . The assumption of a lightly loaded propeller is made, the velocity fluctuations are expressed in blade fixed coordinates for each n-th harmonic component, and the phase shift ϕ_n depends on both the skew angle ψ_j and the blade spacing $\eta_n = 2\pi l/N_b$.

Adding the contributions of the gust velocities to the unsteady lift, and replacing the factor of 2π with the blade section lift curve slope to account for the additional lift due to adjacent blades, one obtains for the lift and moment on a blade section

$$L_{nj} = -\left[\frac{\partial C_L}{\partial \alpha}\right] \rho \tfrac{1}{2} C_j V_{rj} V_n c_{nj}^* \exp(in[\Omega t - \phi_n]) \cdot \left[K(k_{nj})\cos\beta_j - \alpha_j T(k_{nj})\sin\beta_j\right] \Delta r_j \tag{3}$$

$$M_{jn} = L_{jn} r_j \tag{4}$$

where the reduced frequency is $k_{nj} = n\Omega \tfrac{1}{2} C/V_{rj}$. The lift curve slope can be determined experimentally or approximated, for example, by the method of Weinig described in Wislicenus (1965).

As the propeller rotates, blade position dependent x and y components of the lift vector and the moment arm are generated. Therefore, in addition to the thrust and torque, there are x and y force and moment components. Also, it has been shown that the only harmonics contributing to the thrust and torque are those of order mN_b (some multiple of blade number), and the only harmonics contributing to the side forces and moments are of order $mN_b \pm 1$. Since the contributions from the different harmonic groups oscillate at different frequencies they should be considered separately and doing so results in the following expressions for the unsteady forces and moments due to a particular harmonic group m.

$$F_z^{(m)} = N_b \sum_{j=1}^{P} \left[L_{j(mN_b)} \right]_1 e^{-imN_b\psi_j} \tag{5}$$

$$T_z^{(m)} = N_b \sum_{j=1}^{P} \left[M_{j(mN_b)} \right]_1 e^{-imN_b\psi_j} \tag{6}$$

$$F_x^{(m)} = \tfrac{1}{4} N_b \, i \sum_{j=1}^{P} \left\{ \left[L_{j(mN_b+1)} \right]_2 - \left[L_{j(mN_b-1)} \right]_2 \right\} e^{-imN_b\psi_j} \tag{7}$$

$$F_y^{(m)} = \tfrac{1}{4} N_b \sum_{j=1}^{P} \left\{ \left[L_{j(mN_b+1)} \right]_2 + \left[L_{j(mN_b-1)} \right]_2 \right\} e^{-imN_b\psi_j} \tag{8}$$

$$T_x^{(m)} = \tfrac{1}{4} N_b \, i \sum_{j=1}^{P} \left\{ \left[M_{j(mN_b+1)} \right]_2 - \left[M_{j(mN_b-1)} \right]_2 \right\} e^{-imN_b\psi_j} \tag{9}$$

$$T_y^{(m)} = \tfrac{1}{4} N_b \sum_{j=1}^{P} \left\{ \left[M_{j(mN_b+1)} \right]_2 + \left[M_{j(mN_b-1)} \right]_2 \right\} e^{-imN_b\psi_j} \tag{10}$$

In addition to the above forces and moments, Thompson's method was extended (Mautner, 1987b; Mautner and Blaisdell, 1987) to include calculation of the maximum side force and bending moment. Briefly, the forces and moments are expressed in complex form, and, via a coordinate rotation, the derived equations for the total side force and bending moment vector trace an ellipse where the semi-major axis yields the maximum amplitude of the side force and bending moment. The equations are

$$F_s^{(m)} = \tfrac{1}{4} N_b \left| \sum_{j=1}^{P} \left[L_{j(mN_b-1)} \right]_2 e^{-imN_b\psi_j} \right| + \tfrac{1}{4} N_b \left| \sum_{j=1}^{P} \left[L_{j(mN_b+1)} \right]_2 e^{-imN_b\psi_j} \right| \tag{11}$$

$$T_s^{(m)} = \tfrac{1}{4} N_b \left| \sum_{j=1}^{P} \left[M_{j(mN_b-1)} \right]_2 e^{-imN_b\psi_j} \right| + \tfrac{1}{4} N_b \left| \sum_{j=1}^{P} \left[M_{j(mN_b+1)} \right]_2 e^{-imN_b\psi_j} \right| \tag{12}$$

The subscripts 1 and 2 used in the force and moment equations (5)-(12) indicate the following forms of the lift and moment equations

$$\left[L_{jn}\right]_1 = -\left[\frac{\partial C_L}{\partial \alpha}\right]_j \rho^{1/2} C_j V_{ij} V_n c_{nj}^{1/2} \left\{K(k_{ij})\cos\beta_j - \alpha_j T(k_{ij})\sin\beta_j\right\}\Delta r_j \cos\beta_j \tag{13}$$

$$\left[L_{jn}\right]_2 = \left[L_{jn}\right]_1 \tan\beta_j$$
$$\left[M_{jn}\right]_1 = \left[L_{jn}\right]_2 r_j \qquad \left[M_{jn}\right]_2 = \left[L_{jn}\right]_1 r_j \tag{14}$$

where the index n takes on the values mN_b, mN_b+1 or mN_b-1. This completes the formulation of unsteady force and moment equations. A description of the skew optimization method is given in the next section.

SKEW OPTIMIZATION MODEL

To determine the optimum skew distribution the above force calculation method was incorporated into a nonlinear programming problem. Due to the fact that, in general, all forces cannot be minimized simultaneously, a scalar cost function formed from the weighted, linear combination of the forces and moments is minimized. The cost function F_c is

$$F_c = \sum_{m=1}^{4}\left[\frac{W_1^{(m)}F_x^{(m)}}{.05\hat{F}_x} + \frac{W_2^{(m)}F_y^{(m)}}{.05\hat{F}_x} + \frac{W_3^{(m)}T_x^{(m)}}{.05\hat{T}_x} + \frac{W_4^{(m)}T_y^{(m)}}{.05\hat{T}_x}\right] \tag{15}$$

where the weights, $W_j^{(m)}$, are normalized such that their sum over both m and j (=1,....,4) equals 1. The normalization factors (i.e. the steady state thrust and torque, $\hat{F}_x$ and $\hat{T}_x$) are arbitrary; however, the $W_j^{(m)}$ are chosen to place emphasis on the suppression of particular forces or moments.

Since F_c depends upon the skew distribution, $\psi(r)$, one could solve for the optimum skew distribution via a variational or n-dimensional parameter optimization technique. However, a more feasible approach, and the one used here, is to use a few parameters in describing the skew distribution and perform an optimization search in a limited parameter space. To accomplish this, the skew distribution is represented by either a cubic or quadratic distribution having a straight line section with $\psi=0$. The skew distribution (see Geenblatt, 1978; Mautner and Blaisdell, 1987), illustrated in figure 3, is described by

$$\psi(r) = A_1 r^3 + A_2 r^2 + A_3 r + A_4 \quad \text{or} \quad A_2 r^2 + A_3 r + A_4 \qquad r_o \le r \le r_t$$
$$\psi(r) = 0 \qquad r_h \le r \le r_o \tag{16}$$

The skew distribution given above has five free parameters (A_1, A_2, A_3, A_4, r_o); however, it is more meaningful to the propeller designer to use parameters that have physical meaning instead of using these polynomial coefficients. The parameters chosen for use in the current method are the skew at the propeller tip ψ_t, the starting skew slope $S_o = \psi'(r_o)$, the starting radius r_o, and the skew slope at the tip S_t. Additionally, the physical restriction that $\psi(r_o)=0$ is made so that the skew distribution is continuous thereby reducing the number of free parameters by one. Another necessary restriction is that the skew distribution be smooth which implies that $S_h = \partial\psi(r_o)/\partial r = 0$ if $r_o > r_h$. If there is no straight line section $r_o = r_h$, S_h is not restricted but r_o is fixed. In either case, the number of free parameters is reduced to three for a cubic distribution and two for a quadratic distribution and results in the four possible skew distribution models presented in table 3. Specification of these models allows the optimization search to be carried out in either a two- or three-dimensional space.

The propeller skew distribution problem has now been formulated as an optimization problem in terms of a few geometric parameters. In order to obtain a feasible propeller geometry, it is necessary to place some restrictions, such as a maximum allowable tip skew, on the geometric parameters. In doing so, the design problem becomes a constrained, nonlinear optimization problem where the optimization search is restricted to finding the set of parameters which minimizes the cost function F_c while satisfying all of the constraints placed on the problem. The constraints used are given in table 4 and are checked for violation at a given point in the parameter space using the method developed by Greenblatt (1978). The additional constraint that the propeller blade should not curve forward has been added.

The constrained, nonlinear optimization problem is represented by

$$\min\ F_c(\underline{X}) \text{ subject to } G_j(\underline{X}) \ge 0 \tag{17}$$

where $\underline{X}$ is a vector in parameter space which determines the skew distribution and $G_j(\underline{X})$ describes the constraints. There are many techniques for solving the unconstrained minimization problem (see Parsons, 1975); however, only a few methods attack the constrained problem directly. One useful technique is to convert the constrained problem into an unconstrained problem and then use an unconstrained optimization method. This can be accomplished with the use of an external penalty function which is added to a cost function whenever a constraint is violated (i.e. $G_j(\underline{X}) < 0$). The penalty function is

$$Pe(\underline{X}, A_k) = F_c(\underline{X}) - A_k \sum_j \min\left[G_j(\underline{X}), 0\right] \tag{18}$$

An unconstrained optimization technique can be applied to $Pe(\underline{X}, A_k)$. If no constraint is violated no penalty is added and the penalty function is the same as the cost function. Since the penalty added is proportional to the constraint violation, the optimization method should be forced towards a feasible region where no constraints are violated. This will be the case as long as the multiplicative factor A_k is large enough (≈ 1024); however, if A_k is too small, the search may tend toward an infeasible region. The optimization technique chosen for use in this method is the Nelder-Mead simplex search method (Nelder and Mead, 1965), and a detailed description of the method as coded in the current computer program is given by Mautner and Blaisdell (1987).

The computer program which solves the above nonlinear programming problem is an interactive program intended for routine propeller design work. The program has an interactive input method to accept propeller data and optimization parameters, and the program can be restarted, for example, with different constraint values. In addition to the optimization mode, a test mode is available for the calculation of unsteady forces for a given skew distribution.

NUMERICAL EXAMPLES

FOURIER ANALYSIS

In addition to the specification of propeller geometry, a preliminary step in the calculation of unsteady forces and skew distributions is an analysis of the input wake. Examination of the unsteady force equations shows that a Fourier analysis of the wake is required, and that only certain harmonics of the input wake will contribute to the unsteady forces and moments. The Fourier analysis of the current four cycle wake shows that the

harmonic numbers of interest are 4, 8, 12, 16, ... (all others have zero magnitude). Also, since a six bladed propeller is being used in this example, the harmonics of concern include 6, 12, 18, 24, ... Thus for a six bladed propeller operating in a four cycle wake, the only harmonics of interest are 12, 24, 36, ... (If, for example, a seven bladed propeller was specified, one would consider side forces due to harmonics of order $mN_b \pm 1$.) The radial distribution of the Fourier coefficients and phase angles for the 12th and 24th harmonics are given in figures 4, 5 and 6. The results show both the dominance of the 12th harmonic, especially in the region of $r/R_0 < 0.5$, and the rapid approach to a nearly zero magnitude of the 24th and higher harmonics. For example, the peak value of c_n for the 24th harmonic is 2.5 times lower than the peak c_n for the 12th harmonic. The phase angle distributions (figure 6) show that the phase for the 24th harmonic is nearly constant over radius while the phase angle of the 12th harmonic has a nearly constant positive magnitude for $0 < r/R_0 < \approx 0.5$, it undergoes a sharp phase shift at $r/R_0 \approx 0.5$, and then has a nearly constant negative magnitude over $\approx 0.6 < r/R_0 < \approx 0.9$. Finally, since the harmonic numbers of concern are 12, 24, 36, ... the only forces that need to be calculated are the unsteady thrust and torque.

UNSTEADY FORCES

To illustrate use of the unsteady force calculation method, the six bladed propeller geometry and operating parameters (tables 1 and 2) along with the 12th and 24th harmonic distributions were provided as inputs to the method. The calculated radial distributions of F_s and T_s are given in figures 7 and 8 for the 12th and 24th harmonics. The radial distributions for $mN_b=12$ show that regions of large forces occur in both the inner and outer portions of the propeller blade. Also, there is a distinct minimum force region, located at $r/R \approx 0.68$, which coincides with the minimum velocity defect/excess region of $r/R_0 \approx 0.53$ shown in figure 1. The forces for the 24th harmonic are significantly lower that those for 12th harmonic and increase in magnitude with increasing radius. This result follows directly from the lower harmonic magnitudes for $mN_b=24$. Radial distributions of forces such as that shown in figures 7 and 8 provide information relevant to what portion of the wake is most important in the production of unsteady forces and in the possible reduction of these forces by appropriate appendage/vehicle design. A detailed comparison of the wakes behind various appendage geometries and the resulting unsteady forces can be found in Mautner (1987a).

SKEW DISTRIBUTIONS

To demonstrate the types of skew distributions which can be obtained using the current optimization method, the four models summarized in tables 3 and 4 were used to calculate "optimum" skew distributions and the magnitude of the unsteady thrust and torque associated with the skew distributions. To provide a reference, the magnitude of the unsteady thrust and torque for the unskewed propeller was calculated. Next, each of the four skew distribution models, with essentially no limits on the constraints, was specified. For example, the limit on maximum tip skew was $2\pi/N_b$. The calculated unsteady thrust and torques are given in table 5 where the reduction in forces obtained for each skew distribution is represented by $F_s/\bar{F}_s$ and $T_s/\bar{T}_s$ where the bar represents the unskewed values. The calculated skew distributions are plotted in figures 9-11 where the letters correspond to the particular cases listed in table 5.

It is clear from an examination of the calculated forces given in table 5 (cases A, B, C, F) that a significant reduction of the total unsteady thrust and torque was achieved for the 24th harmonic irregardless of the skew distribution model used. However, for the 12th harmonic, the quadratic distributions #1 and #2 (A,B) and the cubic #4 (F) distribution produced significantly less reduction in the magnitude of both the thrust and torque. The largest force reduction, for $mN_b=12$, occurs for cubic #3 (C) which also has a shape (figure 9) that deviates drastically from the general shape of the other three skew distributions (A,B,F). The resulting shape of cubic #3 (C) points out a potential problem with the specification of unlimited constraints. While the method attempts to provide the skew for minimum force reduction, it may provide a skew distribution which is not feasible in terms of final propeller geometry. The results of applying constraints to the cubic #3 model are shown in figure 10. When the starting skew slope is limited, the resulting skew distribution and force reduction fall in line with the results obtained for the other models (figure 9).

As shown by equation (15), the skew optimization problem involves the linear combination of weighted forces. The weights W_j are specified by the propeller designer and thus can be chosen to place more emphasis on the reduction of a particular force in a particular harmonic group. To illustrate the effect of varying the weights W_j the cubic #3 and cubic #4 models were used. In addition to the $W_j=1$ used in the previous calculations, the weights were increased to 5 and 10 for the 12th harmonic while maintaining $W_j=1$ for the 24th harmonic. The results presented in table 5 and figure 11 show very little change in the force magnitudes and the shape of the skew distributions. This result is not surprising due to the dominance of the 12th harmonic magnitude (figures 4 and 5).

As mentioned previously, the original motivation for the introduction of skew into marine propeller design was the reduction of both blade-rate noise and vehicle vibration. The basic idea was to introduce a phase shift in the local periodic lift forces over the radial extent of the blade. The phase shift should be specified such that the local forces, at the inner and outer radii, are acting in opposition. To illustrate the results of applying the force equations to obtain a phase shift, the radial distribution of the real an imaginary parts of unsteady thrust distributions are plotted in figures 12 and 13 for $mN_b=12$. The figures compare the radial distribution of unsteady thrust for the case of no skew with the force distribution obtained using the cubic #3 (C) skew distribution model. The radial distribution of both the real and imaginary parts of F_s demonstrate the acquisition of a phase shift in the unsteady lift by the large changes in magnitude of the unsteady force. Due to the character of the 12th harmonic distribution, it is not possible to obtain a phase shift in the real part of F_s such that the forces at the inner and outer radii are acting in opposition; however, the forces are acting in opposition for the the imaginary part of F_s. The results in figures 12 and 13 show that the forces are shifted from their original condition thus producing, at least, some unsteady force reduction. Similar results are obtained for the unsteady thrust associated with $mN_b=24$ and the unsteady torque (not shown here) for both the 12th and 24th harmonics.

The close similarity in most of the skew distributions (figure 9-11) indicates that satisfactory, but not necessarily optimum, propeller geometries can be obtained without having to place severe restrictions on the skew distribution model constraints. However, the magnitudes of the unsteady forces and moments listed in table 5 demonstrate that for an actual propeller design the effect of parameters such as skew slope and tip skew need to be examined closely for its effect on each harmonic group.

SUMMARY

A propeller skew optimization program, based upon Greenblatt's method, has been developed. The method uses a quadratic or cubic skew distribution model, and a parameter search, subject to constraints, is performed to determine the skew distribution which minimizes a linear combination of the unsteady forces and moments. It should be remembered that this program requires user judgement in the specification of the skew distribution model and constraints.

The two-dimensional, unsteady airfoil theory used in the unsteady force calculation method may not be as accurate as three-dimensional, unsteady lifting-surface methods in predicting unsteady loads (i.e. for low aspect ratio blades). However, if the errors are consistent so that the method predicts the correct trends in the unsteady forces, the resulting skew distribution should be reasonably accurate. It should also be noted that the original intention of incorporating Thompson's (1976) force calculation method into the optimization program was to provide a well documented and efficient method for use, at least, during the development phase of the skew optimization program. Although, Thompson (1976) obtained good agreement between theory and experiment and the current method provides reasonable skew distributions, the need exists for additional program enhancements.

One problem inherent in the application of skew involves the use of wake data obtained without a propeller present. While the propeller design method of Nelson (1972, 1975) calculates changes in the circumferential mean, inflow velocity field due to presence of the propulsor (i.e. induced and interference velocities), the uncorrected, spatially varying inflow is used to determine the unsteady forces. It is known that the presence of a propulsor will cause a change in the streamlines due to acceleration of the flow, that there may be additional unsteadiness due to the relative motion of the blades and that the propeller will change the amplitude and phase of the incident distortion velocity. From these few facts it is apparent that the incident wake should be corrected for propulsor effects.

Attempts are being made to develop unsteady force calculation methods which account for the effects of both the presence of the propulsor and the blade skew on the harmonic content of the incident wake. One such effort is that by Zierke (1985). He has pointed out that both the amplitude and phase angle of the inlet distortion will be modified by the blade skew (warp affects both amplitude and phase and rake affects the amplitude), and that skew is a measure of when a blade section first encounters a disturbance. Zierke has developed an unsteady force calculation method which both accounts for the changes in amplitude and phase of a disturbance due to the presence of a rotating blade and uses leading edge skew rather than mid-chord skew to describe the blade. An obvious improvement to the current method would be the incorporation these kinds of corrections.

ACKNOWLEDGEMENTS

This work was funded by the Torpedo Hydromechanics and Hydroacoustics Program of the Naval Sea Systems Command, the Torpedo Silencing Program of the Naval Underwater Systems Center and the Naval Ocean Systems Center Independent Exploratory Development Program. I thank G. Blaisdell for his work on the original development and programming of the method.

REFERENCES

Greenblatt, J.E., "SKEWOPT: A Propeller Skew Optimization Program, User's and Programmer's Documentation," Univ. of Michigan, Dept. of NAME Report No. 204, 1978.

Horlock, J.H., "Fluctuating Lift Forces on Airfoils Moving Through Transverse and Chordwise Gusts," J. Basic Eng., 1968.

Mautner, T.S., "The Relationship Between Appendage Geometry and Propeller Blade Unsteady Forces," AIAA Paper No. 87-2064, AIAA/SAE/ASME/ASEE 23rd Joint Propulsion Conference, San Diego, CA, 1987a.

Mautner, T.S., "A Propeller Skew Optimization Method," Proc. ICIDES-II, Penn. State Univ., Oct., 1987b.

Mautner, T.S. and Blaisdell G. A., Author's Technical Notes Being Prepared For Publication, 1987.

Metzger, F.B., "The State of the Art in Prop-Fan and Turboprop Noise," AGARD Conference Proceedings No. 366, Aerodynamics and Acoustics of Propellers, Toronto, Canada, 1984.

Metzger, F.B. and C. Rohrbach, "Benefits of Blade Sweep for Advanced Turboprops," J. Propulsion, Vol. 2, No. 6, 1986.

Naumann, H. and H. Yeh, "Lift and Pressure Fluctuations of a Cambered Airfoil Under Periodic Gusts and Applications in Turbomachinery," J. of Eng. and Power, Vol. 95, No. 1, 1973.

Nelder, J.A. and R. Mead, "A Simplex Method for Function Minimization," Computer J., Vol. 7, No. 4, 1965.

Nelson, D.M., Development and Application of a Lifting Surface Design Method for Counterrotating Propellers, NUC TP 326, 1972.

Nelson, D.M., A Computer Program Package for Designing Wake-Adapted Counterrotating Propellers: A User's Manual, NUC TP 494, 1975.

Nelson, D.M. and Fogarty, J.J., Private Communication, 1977.

Parsons, M.G., "Optimization Methods for Use in Computer-Aided Ship Design," Proceedings of the First Ship Technology and Research (STAR) Symposium, Washington, D.C., 1975.

Parsons, M.G. and J.E. Greenblatt, "Optimization of Propeller Skew Distribution to Minimize the Vibratory Forces and Moments Acting at the Propeller Hub," Univ. of Michigan, Dept. of NAME Report No. 206, 1978.

Sears, W.R., "Some Aspects of Non-Stationary Airfoil Theory and Its Practical Application," J. Aero. Sciences, Vol. 8, No. 3, 1941.

Schulten, J.B.H.M., "Aerodynamics of Wide-Chord Propellers in Non-Axisymmetric Flow," AGARD Conference Proceedings No. 366, Aerodynamics and Acoustics of Propellers, Toronto, Canada, 1984.

Takallu, M.A. and P.J.W. Block, "Prediction of Added Noise Due to the Effects of Unsteady Flow on Pusher Propellers," AIAA 87-0255, Jan. 1987.

Thompson, D.E., "Propeller Time-Dependent Forces Due to Nonuniform Flow," Applied Research Laboratory, Pennsylvania State Univ., Tech. Mem. TM No. 76-48, 1976.

Zierke, W.C., "Two-Dimensional, Unsteady Airfoil Theory for the Calculation of Unsteady Forces and Moments in Turbomachinery," Applied Research Laboratory, Pennsylvania State Univ., Tech. Mem. TM 85-28, 1985.

Table 1. Theoretical Performance of the Counterrotating Propeller Set

Propeller radius (in)	R_P=R	8.2
RPM	RPM	1400
Propulsive coefficient	PC	0.925
Thrust deduction factor	t	0.141
Vehicle speed (knots)	V_s	43
Drag coefficient	C_D	0.115
Advance ratio	J	2.12
Blade surface cavitation	σ	0.75
Thrust coefficient	C_T	0.218
Torque coefficient	C_Q	0.137
Blade tip speed	$V_{tip}/V_s)_F$	1.731
	$V_{tip}/V_s)_A$	1.604
Number of blades	$N_{b\cdot F}$ x $N_{b\cdot A}$	6 x 4
Hub radius (in)	r_h	3.44
Body radius (in)	R_B	10.5
Subscripts = F - Forward and A - After Propeller		

Table 2. Propeller Geometry and Operating Characteristics

r/R	½C/D	β	V_{ij}/V_s
0.4344	0.0838	0.5650	0.7200
0.4634	0.0897	0.5913	0.7922
0.4924	0.0953	0.6231	0.8625
0.5214	0.1007	0.6434	0.9297
0.5504	0.1058	0.6594	0.9919
0.5794	0.1106	0.6800	1.0498
0.6084	0.1151	0.7001	1.1038
0.6374	0.1193	0.7128	1.1557
0.6665	0.1231	0.7157	1.2063
0.6955	0.1266	0.7111	1.2555
0.7245	0.1296	0.7025	1.3038
0.7535	0.1321	0.6914	1.3512
0.7825	0.1339	0.6781	1.3979
0.8115	0.1346	0.6624	1.4442
0.8405	0.1333	0.6432	1.4900
0.8695	0.1293	0.6194	1.5363
0.8985	0.1214	0.5907	1.5818
0.9275	0.1090	0.5637	1.6257
0.9565	0.0913	0.5446	1.6688
0.9855	0.0679	0.5185	1.7115

Table 3. Skew Distribution Models.

Model	Type	Free Parameters	Fixed Parameters
1	Quadratic	ψ_t , S_h	$r_s = r_h$
2	Quadratic	ψ_t , r_s	$S_h = 0$
3	Cubic	ψ_t , S_t , S_h	$r_s = r_h$
4	Cubic	ψ_t , S_t , r_s	$S_h = 0$

Table 4. Skew Distribution Constraints

Constraint	Parameters
Skew Start Radius	$r_h \le r_s \le r_t$
Tip Skew	$\psi_{t,min} \le \psi_t \le \psi_{t,max}$
Skew At Any Radius	$\psi_{min} \le \psi(r) \le \psi_{max}$
Start Skew Slope	$S_{h,min} \le S_h \le S_{h,max}$
Slope At Any Radius	$\psi'_{min} \le \psi'(r) \le \psi'_{max}$

Table 5. Calculated Unsteady Force Reduction and Tip Skew.

Skew Model (see Table 3)	mN_b=12 F_z^*	mN_b=12 T_z^*	mN_b=24 F_z	mN_b=24 T_z	Skew ** ψ_t	W_R
No Skew	38.1	12.8	13.4	5.4	0.0	1
	$F_z/\bar{F}_z^{\#}$	$T_z/\bar{T}_z^{\#}$	$F_z/\bar{F}_z$	$T_z/\bar{T}_z$		
No Skew	1.00	1.00	1.00	1.00	0.0	1
(A) Quadratic *1	0.70	0.55	0.17	0.07	59.6	1
(B) Quadratic *2	0.65	0.52	0.25	0.17	57.4	1
(C) Cubic *3	0.09	0.19	0.09	0.07	58.6	1
(D) Cubic *3+	0.31	0.21	0.14	0.11	59.7	1
(E) Cubic *3++	0.42	0.29	0.15	0.11	59.1	1
(F) Cubic *4	0.50	0.37	0.13	0.07	59.8	1
(G) Cubic *3	0.08	0.02	0.11	0.09	59.5	5
(H) Cubic *3	0.08	0.02	0.11	0.09	59.5	10
(I) Cubic *4	0.39	0.26	0.12	0.09	59.6	5
(J) Cubic *4	0.42	0.29	0.14	0.09	59.2	10

Constraints
Tip Skew - Max = 60° and Min = −30°
Maximum/Minimum Skew Slope - ±5.28
Start Radius - r_h=3.44 in

Notes
* Units (F)orce (thrust)-lbs; (T)orque-ft-lbs
** Mid-chord tip skew - deg
\# Bar indicates no skew thrust and torque
\+ Starting slope constraint - $-1 \le S_0 \le +1$
++ Starting slope constraint - $-0.25 \le S_0 \le +0.25$

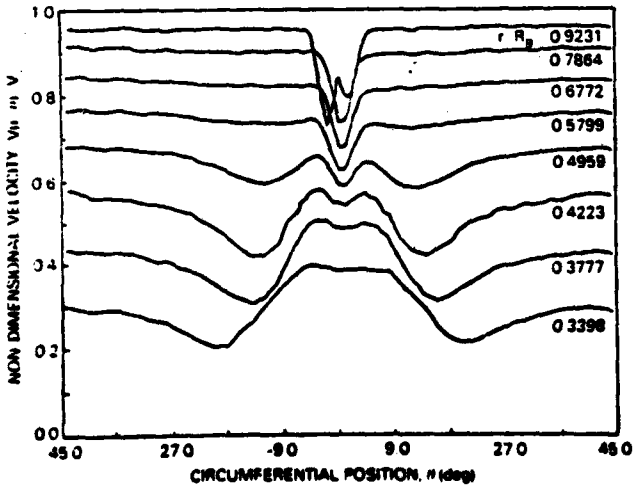

Figure 1. Circumferential Variation of the Inflow Velocity Field.

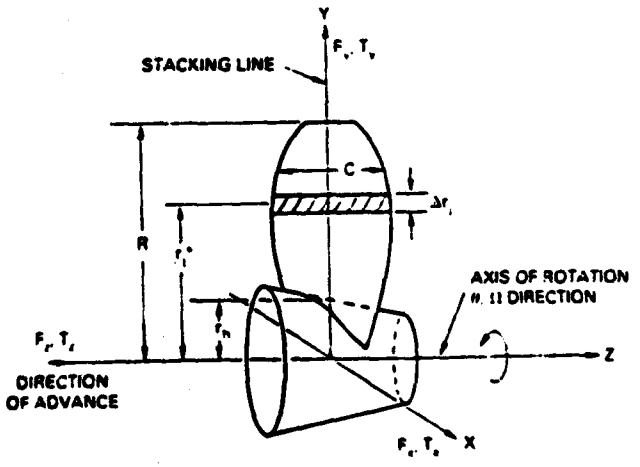

Figure 2. Description of a Typical Propeller and its Geometry.

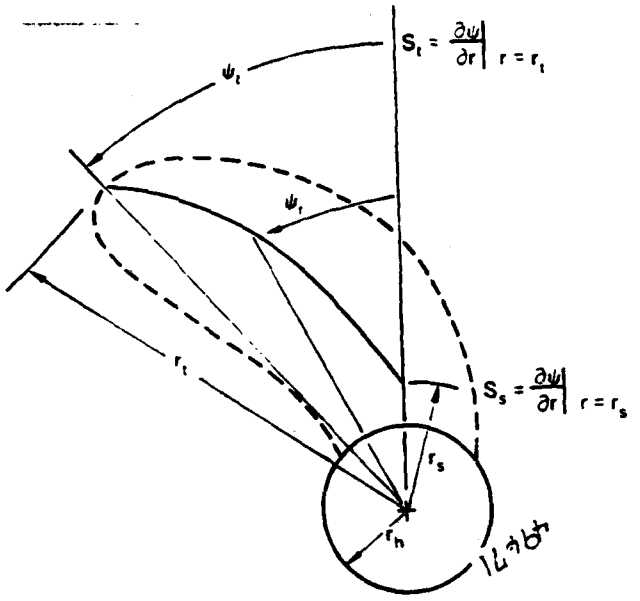

Figure 3. Definition of the Skew Distribution Model Parameters.

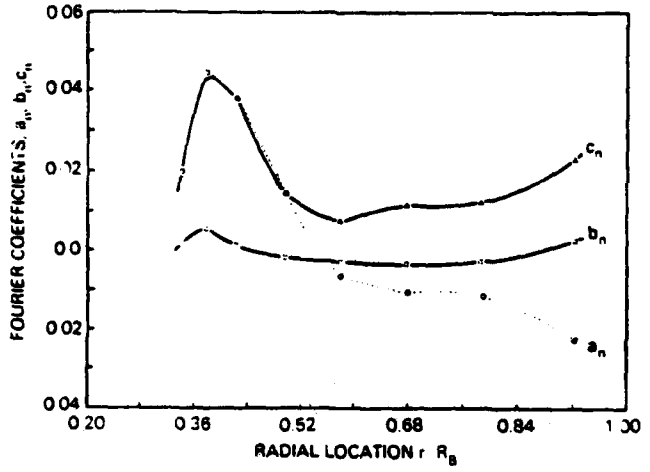

Figure 4. Variation of Fourier Coefficient Amplitude With Radial Position for the 12th Harmonic.

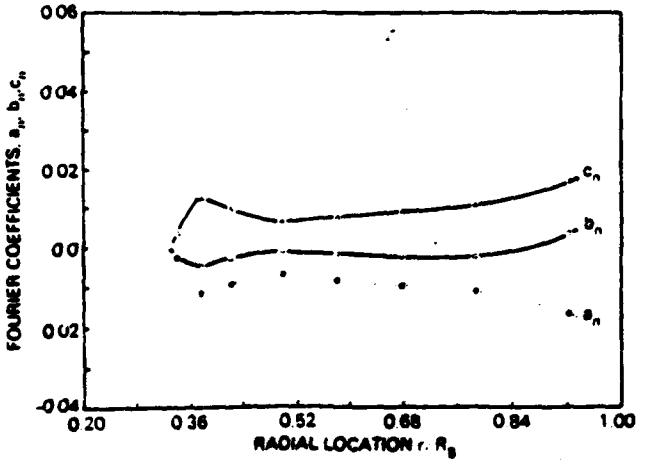

Figure 5. Variation of Fourier Coefficient Amplitude With Radial Position for the 24th Harmonic.

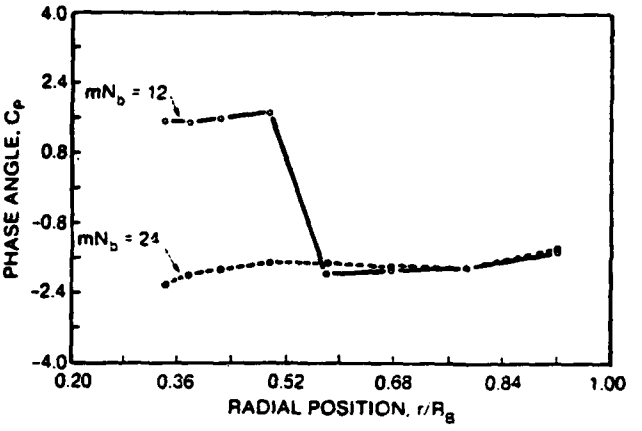

Figure 6. Variation of the Fourier Coefficient Phase Angle with Radial Position for the 12th and 24th Harmonics.

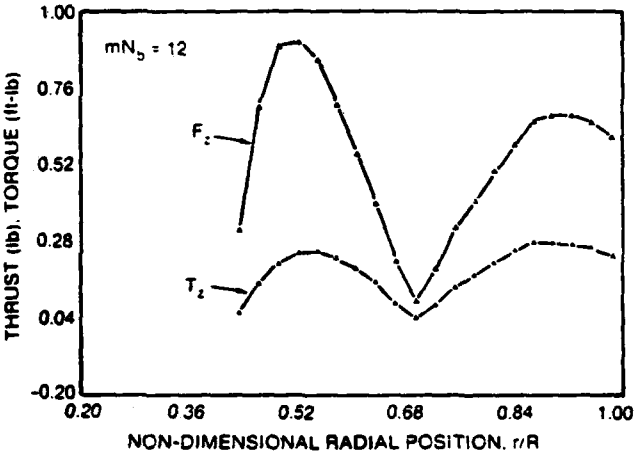

Figure 7. Variation of the Unsteady Thrust and Torque with Radial Position for the 12th Harmonic.

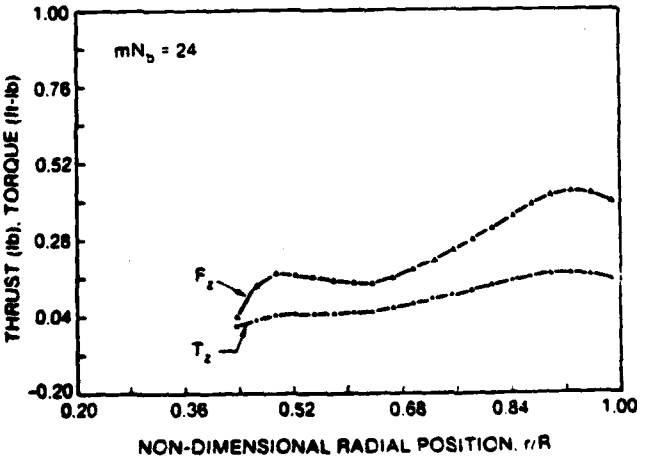

Figure 8. Variation of the Unsteady Thrust and Torque with Radial Position for the 24th Harmonic.

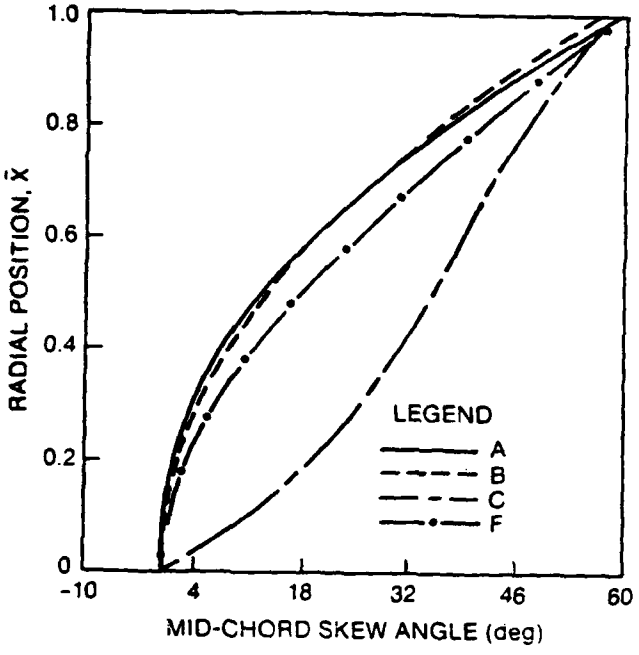

Figure 9. Calculated Mid-Chord Skew Distributions.

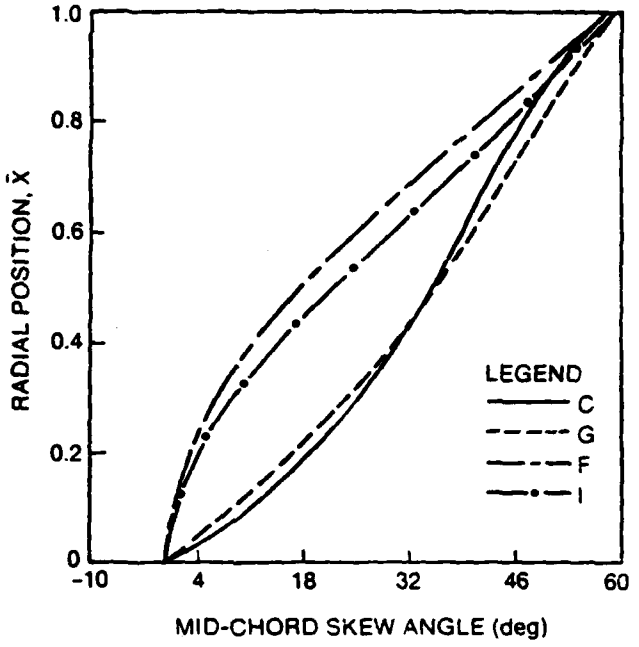

Figure 11. Calcuated Mid-Chord Skew Distributions Using the Cubic #3 and #4 Models for Various Values of the Weighting Function.

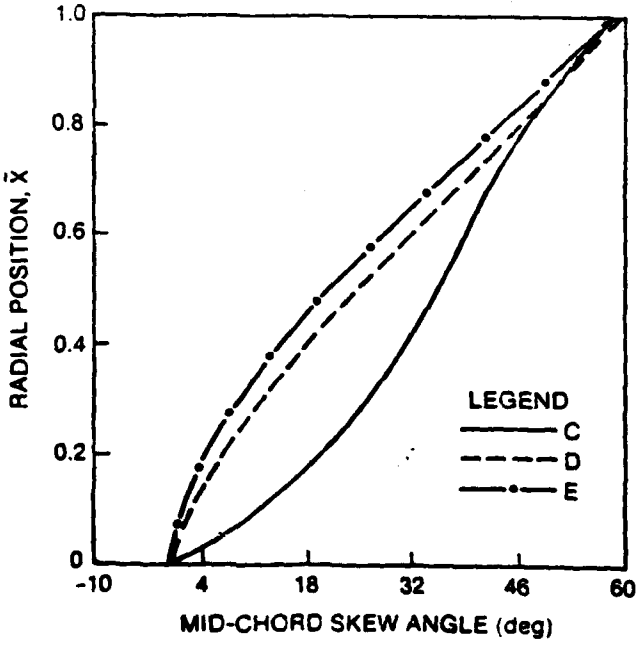

Figure 10. Calculated Mid-Chord Skew Distributions Using the Cubic #3 Model With Various Constraints.

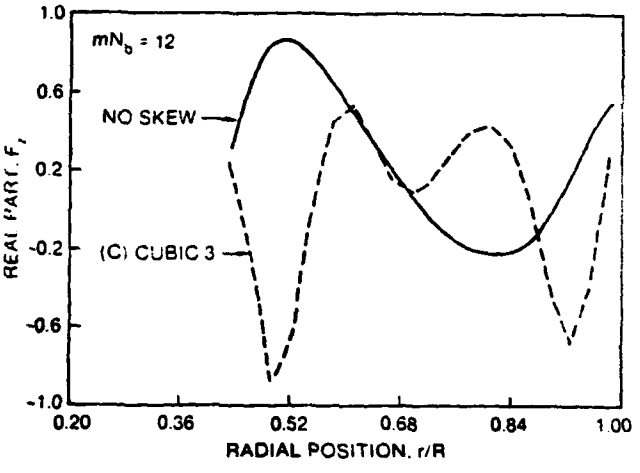

Figure 12. Variation of the Real Part of the Unsteady Thrust with Radial Position for the 12th Harmonic.

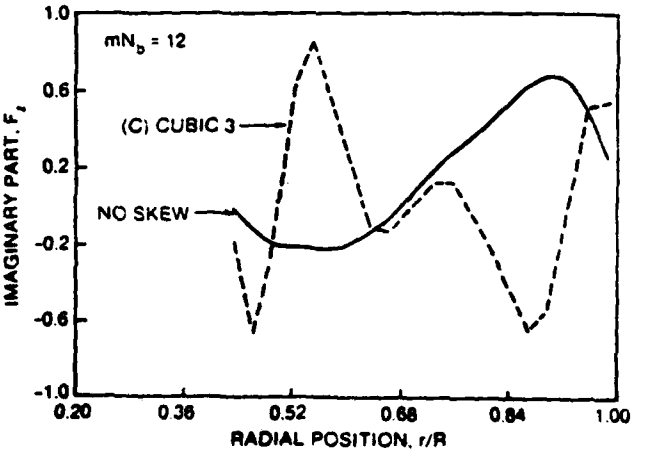

Figure 13. Variation of the Imaginary Part of the Unsteady Thrust with Radial Position for the 12th Harmonic.

END

DATE

FILMED

6-88

DTIC